Electronic Supplementary Material (ESI) for Catalysis Science & Technology.

Electronic Supplementary Information

Selectivity of the Lindlar catalyst in alkyne semi-hydrogenation: a direct liquid-phase adsorption study

Nikolay Cherkasov[1,2*], Dmitry Yu. Murzin[3], C. Richard A. Catlow[4,5], Arunabhiram Chutia[6]

[1] School of Engineering, University of Warwick, Coventry, CV4 7AL, United Kingdom
[2] Stoli Catalysts Ltd, Wellesbourne Campus, Wellesbourne, Coventry, CV35 9EF, United Kingdom
[3] Laboratory of Industrial Chemistry and Reaction Engineering, Process Chemistry Centre, Åbo Akademi University, FI-20500, Turku/Åbo, Finland
[4] School of Chemistry, Cardiff University, Main Building, Park Place, Cardiff, Wales, United Kingdom
[5] Department of Chemistry, University College London, 20 Gordon Street, London, WC1 HOAJ, United Kingdom
[6] School of Chemistry, Brayford Pool University of Lincoln, Lincoln, LN6 7TS, United Kingdom
corresponding author: n.cherkasov@warwick.ac.uk

SI1. Detailed description of the experimental procedures

SI1.1. Details on the adsorption studies

Because of high adsorption constants observed (~10^4 L mol^{-1}) and low adsorption capacity (~ 1 nmol per 50 mg sample), we had to work with low concentrations close to the analytical detection limits.

The system used for adsorption experiments is presented in Figure S1 contains a fraction collector and a syringe pump. The fraction collector had a built-in 3-way valve with a needle that allowed injecting a given solution into any vial. The syringe pump equipped with an SGE 1mL precision syringe acted as a liquid handling unit injecting pre-defined volumes of the solution into vials.

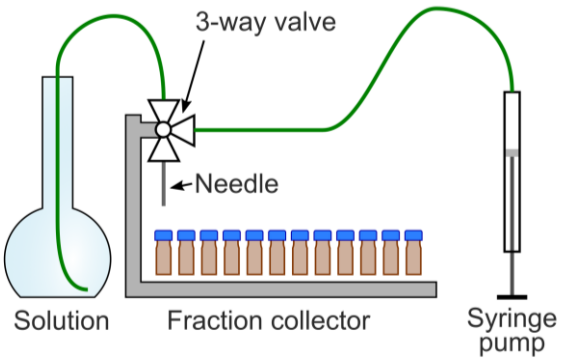

Figure S1. Scheme of the automated system used for the adsorption experiments.

The solution was changed following the procedure of blowing air into all connecting tubes and the syringe, washing with the solvent, and blowing air. Afterwards, 5 full injections into an empty vial were performed to wash the needle. Solutions were changed in increasing concentration order starting from solvent (hexane, 99%, Fischer Scientific).

The vials for the adsorption experiment were divided into 4 parts: (i) control, (ii) reference, (iii) catalyst support, and (iv) catalyst. The control vials were injections of the solvent at the beginning and end of every run. This way, it was possible to control that the solution concentration was consistent during the injection and observe any problems of dead volume in the fluidics connections which would cause a lower concentration at the beginning of the experiment. The remaining three groups of vials contained the same volumes of the solutions. The reference vials were empty to study linearity of the response with the concentration. The vials with 50 mg catalyst support were used to study the adsorption of the compounds over the catalyst support considering that its surface area was significantly higher than that observed for the Pd nanoparticles. Lastly, the vials with 50 mg catalyst were used to study adsorption over both the Pd catalyst and the support.

The vials with the catalyst support and the catalysts were reduced in a flow of 20 mL min^{-1} 5 vol% H_2 in N_2 at 150 ^oC for 1 h followed by flushing with N_2 and passivation with 1 vol% O_2 in N_2 before exposure to air. The adsorption experiments were performed within 2-4 h after exposure to air. A significant decrease in adsorption capacity was observed only after about 1 week of exposure to air.

Analysis of the samples obtained

The samples obtained were analysed directly by gas chromatography with a Shimadzu GC 2010 equipped with an FID detector. High adsorption observed required using trace substance concentrations (~ 0.1 ppm_w) to determine the adsorption parameters. The GC analysis was optimised to ensure high reproducibility and low detection limits. The GC was equipped with a Stabilwax 60 m x 0.32 mm x 1 µm column, 8 µL of the sample were injected in a splitless mode at the column temperature of 40 ^oC and the inlet pressure of 100 kPa. After 4 minutes at 40 ^oC, the column temperature was ramped at 15 $^oC\ min^{-1}$ to 175 ^oC followed by holding this temperature for 3 min. The injector pressure was also ramped after 8.5 min from injection – 30 kPa min^{-1} till 220 kPa followed by holding the pressure for 4.5 min.

The analysis method was extended when quinoline was injected. After reaching the column temperature of 175 ^oC, the second ramping state was started at 25 $^oC\ min^{-1}$ till 255 ^oC. Meanwhile, the injection pressure was also ramped after 8.5 min at 100 kPa – the ramping at 30 kPa min-1 till 380 kPa was performed to desorb quinoline faster.

The method provided a detection limit of 0.2 µM with complete separation of all the studied compounds. The analysis was performed based on the absolute area of the peak corresponding to the repeatability of ± 2%. No internal standard was used to avoid interference with the adsorption such as displacement of the analysed species or adsorption of the internal standard itself.

Analysis of the data obtained

The concentrations in the reference solutions were processed using a weighted least-squares method. The weights were taking into account the experimental error of ±2% or a fixed error (whichever is larger). The fixed error was found to depend on the concentration of the species analysed and varies between 3 μM (when 500-800 μM MBY solution was used), 1 μM when 200 μM MBY or MBE solutions were used, or 0.3 μM when 40 μM MBE solution was taken.

Comparison of the amount of the substrate injected into the vials and determined by the analysis provided the amounts of adsorbed and equilibrium concentrations. These raw data were analysed using the Monte-Carlo regression method [1]. Sets of simulated experimental data (1000 for each case) were created (with errors introduced with a normal distribution and standard deviations as above). These data were fit with the Langmuir adsorption model analysing the parameters obtained statistically considering covariations of the parameters and reporting 90% confidence intervals.

SI1.2. Details on the Computational Modelling

We used the Vienna Ab Initio Simulation Package (VASP) to perform spin-polarised periodic density functional theory-based calculations using the projector augmented wave method [2–5]. The cut-off energy for the expansion of the plane-wave basis sets was set to 550 eV, which gave bulk energies converged to within 10^{-5} eV. For the structural optimization, the convergence criterion was set to 0.01 eV $Å^{-1}$. The ideal Pd(111), Pd(110), and Pd(210) surfaces were modelled by 4x4 cell with 5 atomic layers and of the five atomic layers bottom three layers were fixed to mimic the bulk of the material. The calculated Pd lattice constant of 3.904 Å agreed with the experimental value of 3.891 Å [6].

The adsorption of MBY and MBE molecules on Pd surfaces was allowed only on one of the exposed surfaces and the spurious dipole moment, due to the adsorbed molecule on one of the two surfaces was taken into account using methods implemented in VASP according to the procedures of Makov *et al*. and Neugebauer *et al*.[7,8]. For the interaction of MBY and MBE with Pd surfaces, the dispersive effects may be significant; therefore, in all the calculations, we included Grimme's dispersion correction (DFT+3) [9]. To choose an appropriate k-point grid for these calculations we performed benchmark calculations on the adsorption property of MBY on Pd(111) surface with 3x3x1 and 5x5x1 K-point grid, which yielded a difference in adsorption energy of 7.690×10^{-4} eV, which is within the DFT errors. Additionally, our previous studies on the interaction of organic molecules such as furfural on Pd surfaces have shown that the use of a K-point grid of 3x3x1 was sufficient, therefore, in this study, a K-point grid of 3x3x1 was used [10]. The adsorption energy was calculated as a difference in the total energy of the molecule on the surface and the energies of the isolated molecule and the pristine surface.

SI1.3. Details on kinetic studies and characterisation

Catalyst preparation

The catalyst, 2 wt% Pd/$CaCO_3$ catalyst was prepared by wet impregnation – a solution of palladium (II) acetate (98% Fisher Scientific) was dissolved in acetone and impregnated into the $CaCO_3$ support (99%, Sigma-Aldrich) to provide the Pd loading of 2 wt%. Acetone was evaporated in a rotavapour and the solid material was calcined at 400 ^oC in the flow of air for 1 hour, 100 mL min^{-1}. (All gas flow rates in the work are referred to normal conditions of temperature and pressure). Afterwards, the catalyst was reduced in a flow of 20 mL min^{-1} 5 vol% H_2 in N_2 at 150 ^oC for 1 hour, gas was replaced with N_2 and a small amount of air (1 vol% O_2) was introduced to passivate the catalyst surface.

The Pd catalysts obtained was separated into two parts. One part was poisoned with Pb by mixing the 11 g of the catalyst with 50 mL of 50 mM lead (II) nitrate solution on stirring and heating to about 70 ^oC. The catalyst was decanted from the solution, washed with water (3 x 15 mL) and dried at 70 ^oC.

Catalyst characterisation

Elemental analysis performed on a Rigaku Primus IV WD-XRF instrument using a fundamental parameters model. For the powder experiments, the samples were mounted on a filter paper holder and the weight/diameter used to correct the model for thickness effects. The original Pd catalyst was found to contain 2.1 wt% Pd balance $CaCO_3$ and below 0.05 wt% other elements; the Pd-Pd catalyst contained 1.8 wt% Pd and 3.7 wt% Pb.

CO chemisorption studies were performed in a modified flow adsorption system described in reference [11]. The catalysts (500 mg) were placed into a glass tube between quartz wool plugs. After the reduction at 350 ^oC for 2 h in a flow of 1 vol% H_2 in He 5 mL min^{-1}, purging with He for 2 h and cooling to 35 ^oC, a flow of 4 mL min^{-1} 1.2 vol% CO/ 1.2 vol% Ar in He was admitted into the catalyst with the outlet concentration monitored with a quadrupole mass-spectrometer (m/z=12 to avoid interference with traces of N_2). The CO chemisorption capacity was measured related to the signal of Ar and checked against a reference 0.5 wt% Pt/Al_2O_3 catalyst (provided by Micromeritics). The resulting CO chemisorption capacity for the Pd/$CaCO_3$ catalyst was 4.62±0.12 μmol g^{-1}_{cat} and 2.56±0.10 μmol g^{-1}_{cat} for the Pd-Pb/$CaCO_3$ catalyst.

Liquid-phase hydrogenation

Hydrogenation experiments were carried out in a Parr 160 mL autoclave. In a typical experiment, the catalyst (50 mg) was placed into the reactor and 90 mL hexane (95%, Sigma-Aldrich) solvent was added. The reaction mixture was heated to the desired temperature, purged 5 times with N_2, then 5 times with H_2. The substrate, 2-methyl-3-butyn-2-ol (98%, Fisher Scientific) diluted to 10 mL was added into a separate vessel, degassed purging 5 times with H_2 and injected into the reaction vessel. Reaction time started and the liquid samples (0.7 mL) were collected periodically during the reaction.

The samples collected were analysed with a Shimadzu GC 2010 gas chromatograph equipped with a Stabilwax 10 m x 0.15 mm x 0.15 µm column and a flame ionisation detector. The analysis was performed referring to the internal standard, nonane (98%, Sigma-Aldrich), added into the solvent before the reaction. Experiments with various catalyst masses confirmed the absence of external mass transfer limitations at the stirring rate above 700 rpm. Calculation of the Weisz-Prater numbers showed that internal mass transfer was not a limiting factor.

SI2. Detailed description of the kinetic models used

SI2.1. Model1. Langmuir-Hinshelwood model of non-competitive adsorption of organic species and H_2 over the Pd catalysts.

Figure S2 shows the reaction network of the reactions used in model 1. Here, we use 3 reactions: (i) MBY to MBE, (ii) MBE to MBA, and (iii) direct MBY to MBA. The model assumes non-competitive adsorption of the organic species and hydrogen molecules, which is reasonable considering much larger dimensions of the organic molecules and a large amount of space in between the molecules. In this model, we neglect dimer formation which was below 0.2% compared to either specie – well in agreement with literature data [12].

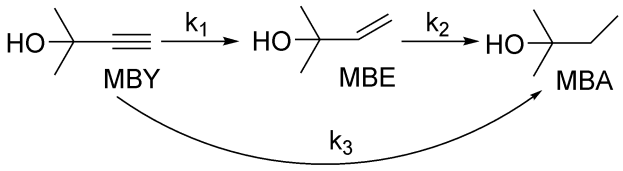

Figure S2. Reaction network of model 1 of MBY hydrogenation reactions.

The elementary steps of the reactions considering adsorption sites for organic molecules (σ) and hydrogen (ϵ) are shown in Table S1.

Table S1. Stages and mathematical expressions corresponding to model 1.

Overall reaction stage	Reaction / process	Mathematical description
H_2 (g) → H_2 (catalyst)	H_2 (gas) $\overset{H}{\leftrightarrow}$ H_2 (solution)	$H = \frac{C_{H2}}{p_{H2}}$
	H_2 (solution) + ϵ $\overset{K_{H2}}{\longleftrightarrow}$ H_2· ϵ	$K_H = \frac{\theta_{\epsilon\,\mathrm{H2}}}{C_{H2}\,\theta_\epsilon}$
MBY → MBE	MBY + σ $\overset{K_{MBY}}{\longleftrightarrow}$ MBY·σ	$K_{MBY} = \frac{\theta_{\sigma MBY}}{C_{MBY}\,\theta_\sigma}$
	MBY·σ + H_2· ϵ $\overset{k_1}{\rightarrow}$ MBE·σ + ϵ	$r_1 = k_1\,\theta_{\sigma MBY}\,\theta_{\epsilon\,\mathrm{H2}}$
MBE → MBA	MBE·σ $\overset{K_{MBE}}{\longleftrightarrow}$ MBE + σ	$K_{MBE} = \frac{\theta_{\sigma MBE}}{C_{MBE}\,\theta_\sigma}$
	MBE·σ + H_2· ϵ $\overset{k_2}{\rightarrow}$ MBA·σ + ϵ	$r_2 = k_2\,\theta_{\sigma MBE}\,\theta_{\epsilon\,\mathrm{H2}}$
	MBA·σ $\overset{K_{MBA}}{\longleftrightarrow}$ MBA + σ	$K_{MBA} = \frac{\theta_{\sigma MBA}}{C_{MBA}\,\theta_\sigma}$
MBY → MBA	MBY·σ + H_2· ϵ $\overset{K_3^*}{\leftrightarrow}$ MBE*·σ + ϵ	$K_3^* = \frac{\theta_{\sigma MBE*}\,\theta_\epsilon}{\theta_{\sigma MBY}\,\theta_{\epsilon\,\mathrm{H2}}}$
	MBE*·σ+ H_2· ϵ $\overset{k_3}{\rightarrow}$ MBA·σ + ϵ	$r_3 = k_3\,\theta_{\sigma MBE*}\,\theta_{\epsilon\,\mathrm{H2}}$

Considering the material balance of the σ and ϵ adsorption sites, free coverage of these sites can be calculated according to equations S1, S2:

$$\theta_\epsilon = \frac{1}{1+K_H\,C_{H2}} = \frac{1}{1+H\,p_{H2}\,K_H}, \qquad (S1)$$

$$\theta_\sigma = \frac{1}{1+K_{MBY}\,C_{MBY}+K_{MBE}\,C_{MBE}+K_{MBA}\,C_{MBA}}. \qquad (S2)$$

Using these equations, coverage of the organic species (MBX = MBY, MBE, or MBA) can be calculated using equation S3:

$$\theta_{MBX} = \frac{K_{MBX}C_{MBX}}{1+K_{MBY}\,C_{MBY}+K_{MBE}\,C_{MBE}+K_{MBA}\,C_{MBA}}. \qquad (S3)$$

The resulting rate equations are shown in equations S4-S6:

$$r_1 = k_1\frac{K_{MBY}C_{MBY}}{1+K_{MBY}\,C_{MBY}+K_{MBE}\,C_{MBE}+K_{MBA}\,C_{MBA}}\cdot\frac{K_H\,H\,p_{H2}}{1+H\,p_{H2}\,K_H}, \qquad (S4)$$

$$r_2 = k_2\frac{K_{MBE}C_{MBE}}{1+K_{MBY}\,C_{MBY}+K_{MBE}\,C_{MBE}+K_{MBA}\,C_{MBA}}\cdot\frac{K_H\,H\,p_{H2}}{1+H\,p_{H2}\,K_H}, \qquad (S5)$$

$$r_3 = k_3K_3^*\frac{K_{MBY}C_{MBY}}{1+K_{MBY}\,C_{MBY}+K_{MBE}\,C_{MBE}+K_{MBA}\,C_{MBA}}\cdot\frac{K_H\,H\,p_{H2}}{1+H\,p_{H2}\,K_H}. \qquad (S6)$$

Considering operation at constant pressure, neglecting MBA adsorption ($K_{MBA} \ll K_{MBE}$) and considering low hydrogen adsorption ($H\ p_{H2}\ K_H \ll 1$), the rate equations can be simplified into equations S7-S9:

$$r_1 = k_1{}' \frac{C_{MBY}}{1+K_{MBY}\ C_{MBY}+K_{MBE}\ C_{MBE}}, \quad (S7)$$

$$r_2 = k_2{}' \frac{C_{MBE}}{1+K_{MBY}\ C_{MBY}+K_{MBE}\ C_{MBE}}, \quad (S8)$$

$$r_3 = k_3{}' \frac{C_{MBY}}{1+K_{MBY}\ C_{MBY}+K_{MBE}\ C_{MBE}}. \quad (S9)$$

where $k_1' = k_1\ K_H\ H\ K_{MBY}\ p_{H2}$, $k_2' = k_2\ K_H\ H\ K_{MBE}\ p_{H2}$, and $k_3' = k_3\ K_3^*\ K_H\ H\ K_{MBY}\ p_{H2}$.

The experimental concentration profiles were integrated with an in-house program written in Matlab using consumptions of the reaction species shown in equations S10-S12:

$$\frac{dC_{MBY}}{dt} = \frac{m_{cat}\ \omega_{Pd}}{V_L\ M_{Pd}}\ (-r_1 - r_3), \quad (S10)$$

$$\frac{dC_{MBE}}{dt} = \frac{m_{cat}\ \omega_{Pd}}{V_L\ M_{Pd}}\ (r_1 - r_2), \quad (S11)$$

$$\frac{dC_{MBA}}{dt} = \frac{m_{cat}\ \omega_{Pd}}{V_L\ M_{Pd}}\ (r_2 - r_3), \quad (S12)$$

where V_L is the total volume of liquid in the reactor, m_{cat} is mass of the catalyst added, ω_{Pd} is mass loading of Pd in the catalyst, and M_{Pd} is the molar mass of Pd metal. The system of these 3 equations was integrated numerically, not considering the material balance of organic species to identify low-accuracy integrations by deviations from the material balance. Figure S3 shows that the values differing by more than a factor of 3 can be obtained fitting *the same* experimental data with high accuracy – the sum of differences between the models based on the k_1 values of $0.3 \cdot 10^8$ L mol_{Pd}^{-1} s^{-1} and $1.1 \cdot 10^8$ L mol_{Pd}^{-1} s^{-1} is vanishingly low!

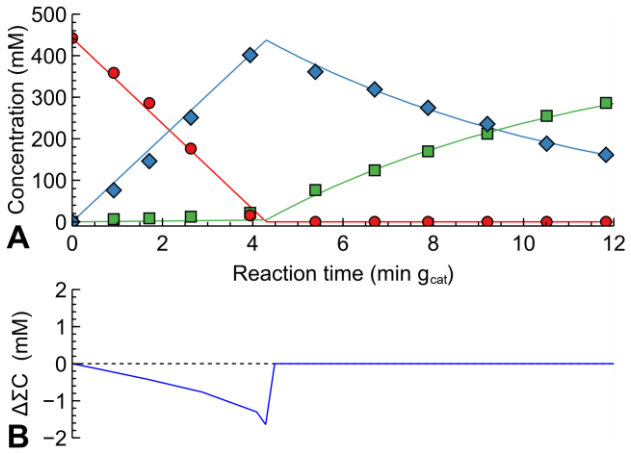

Figure S3. (A) Concentration profile of MBY semi-hydrogenation over a 0.1 wt% Pd/$CaCO_3$ catalyst with the lines corresponding to various Langmuir-Hinshelwood model fitting with (B) differences in all concentration between the models.

Why the results are so ambiguous?

The problem with the results comes from the form of equations S7-S9 and the fact that adsorption is strong. Strong adsorption in mathematical terms means that $K_{MBY}\ C_{MBY} \gg 1$. Taking equation S7 as an example, we could extract $K_{MBY}\ C_{MBY}$ from the denominator to obtain equation S13:

$$r_1 = \frac{k_1'}{K_{MBY}\ C_{MBY}}\ \frac{C_{MBY}}{1/K_{MBY}\ C_{MBY}+1+K_{MBE}\ C_{MBE}/K_{MBY}\ C_{MBY}}, \qquad (S13)$$

In this equation, it is clear that $1/K_{MBY}\ C_{MBY}$ is a vanishingly small value that could be neglected resulting in equation S14:

$$r_1 = \frac{k_1'}{K_{MBY}\ C_{MBY}}\ \frac{C_{MBY}}{1+K_{MBE}\ C_{MBE}/K_{MBY}\ C_{MBY}}, \qquad (S14)$$

It could be simplified eliminating C_{MBY} to obtain equation S15:

$$r_1 = \frac{k_1'}{K_{MBY}}\ \frac{1}{1+K_{MBE}/K_{MBY}\cdot C_{MBE}/C_{MBY}}, \qquad (S15)$$

As a result, there are only 2 independent parameters (k_1'/K_{MBY} and K_{MBE}/K_{MBY}) in the equation. For example, the triplets of (k_1', K_{MBE}, K_{MBY}) of (1,2,1) and (100,200,100) will generate exactly the same k_1'/K_{MBY} and K_{MBE}/K_{MBY} ratios and the same reaction rate in equation (S15) – hence equations S7-S9. Therefore, it is the notation of equations S7-S9 creates a problem and leads to poorly defined results.

SI2.2. Model2. Simplification of model 1 considering relative adsorption constants.

Model 2 considers difficulties in determining the absolute values of the adsorption constants. Relative constants were uses relative adsorption constants for a specie *X* ($Q_X=K_X/K_{MBY}$) *as in equations S16-S18:*

$$r_1 = k_1'' \frac{C_{MBY}}{1/K_{MBY} + C_{MBY} + Q_{MBE}\, C_{MBE}}, \quad (S16)$$

$$r_2 = k_2'' \frac{C_{MBE}}{1/K_{MBY} + C_{MBY} + Q_{MBE}\, C_{MBE}}, \quad (S17)$$

$$r_3 = k_3'' \frac{C_{MBY}}{1/K_{MBY} + C_{MBY} + Q_{MBE}\, C_{MBE}}, \quad (S18)$$

where k_i'' are the corresponding constants k_i' divided by K_{MBY} excluding $k_2'' = k_2\, K_H\, H\, p_{H2}$, K_{MBE} was taken out to form Q_{MBE} into the dividend. If the adsorption constant K_{MBY} is high, the value of $1/K_{MBY}$ can be neglected providing equations S19-S20 used in model 2.

$$r_1 = k_1'' \frac{C_{MBY}}{C_{MBY} + Q_{MBE}\, C_{MBE}}, \quad (S19)$$

$$r_2 = k_2'' \frac{Q_{MBE}\, C_{MBE}}{C_{MBY} + Q_{MBE}\, C_{MBE}}, \quad (S20)$$

$$r_3 = k_3'' \frac{C_{MBY}}{C_{MBY} + Q_{MBE}\, C_{MBE}}, \quad (S21)$$

SI3. Experiments on alkyne displacement with alkene

In a set of experiments, we aimed to verify another basis of the typical Langmuir-Hinshelwood hydrogenation model based on thermodynamic explanation of selectivity – displacement of alkene species with alkyne. An excess of MBE was added to provide full MBE adsorption onto the catalysts before the addition of small amounts of MBY. Figure S4A, B show that there was no appreciable decrease in MBY adsorption over both catalysts studied. The experimental points laid around (and never substantially below) the isotherms observed for the individual components shown as solid lines in the figures. Unfortunately, the attempts to study MBY displacement in presence of high-concentration (~ 1mM) MBE were unsuccessful because trace MBY impurities in the high-concentration MBE solution prevented any adsorption measurements. The existing data, however, indicate that MBE did not displace MBY from the catalyst surface, in agreement with the thermodynamic explanation.

Figure C, D show an experiment that studied if MBE can be displaced with MBY. Here, no significant change in MBE concentration over the catalysts was observed when increasing amounts of MBY were added to the catalyst. Little difference was found on the sequence of dosing the substrates: the addition of either MBY or MBE first resulted in insignificant changes in MBE concentration over the catalysts.

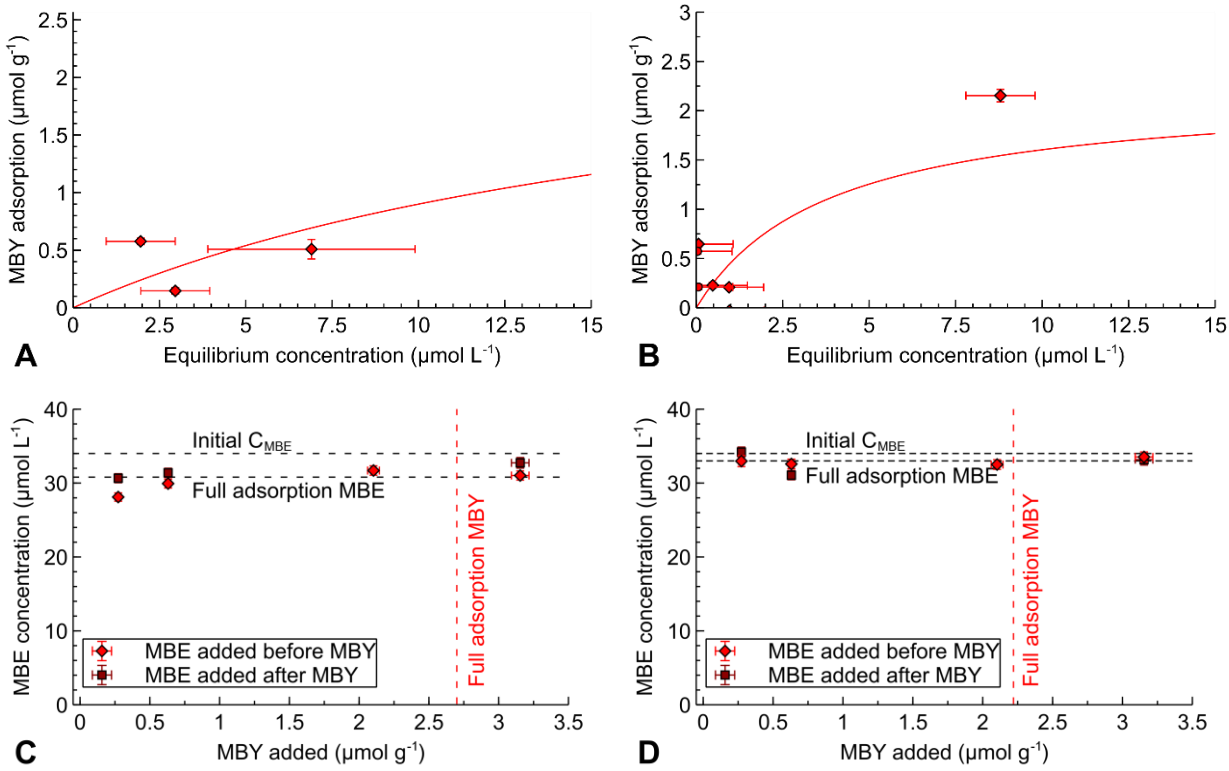

*Figure S4. MBY adsorption over the (A) 2 wt% Pd/$CaCO_3$ and (B) Pb-poisoned 2 wt% Pd/$CaCO_3$ catalysts with pre-adsorbed MBE at the initial concentration of 34 μmol L^{-1}. Solid lines represent adsorption isotherms observed **without** MBE added. Change in equilibrium MBE concentration with MBY addition onto the (C) 2 wt% Pd/$CaCO_3$ and (D) Pb-poisoned 2 wt% Pd/$CaCO_3$ catalysts compared to initial MBE concentration (dashed line).*

Therefore, we can conclude that there are two sites over the Pd catalysts: (i) alkyne sites that strongly adsorb alkyne molecules and weakly alkene molecules, (ii) alkene sites that strongly adsorb only alkenes. The alkene sites do not seem to displace adsorbed alkene species by the excess of alkyne creating a pathway for non-selective reaction. Poisoning the surface of Pd catalyst with Pb significantly decreases the number of alkene adsorption sites – the relative decrease agrees with the corresponding alkyne semi-hydrogenation selectivity.

SI4. Adsorption isotherm of quinoline over the Pd catalysts

Figure shows quinoline adsorption over the 2 wt% Pd/$CaCO_3$ catalyst and Langmuir data fitting. This isotherm shows good agreement with the Langmuir adsorption model. It is worth noting, however, that good fit of the experimental data does not confirm that all model assumptions are valid [13–15]. In particular, we cannot estimate the adsorption energy which may depend on the surface coverage as known in the gas-phase adsorption studies of ethylene and acetylene over the Pd catalysts [16]. Temkin isotherm may be a better fit of the alkyne adsorption over the Pd catalysts and it is possible to speculate that Pb poisons high-energy sites of Pd catalyst. Such speculations, however, are difficult to support further; therefore, Langmuir model was used throughout.

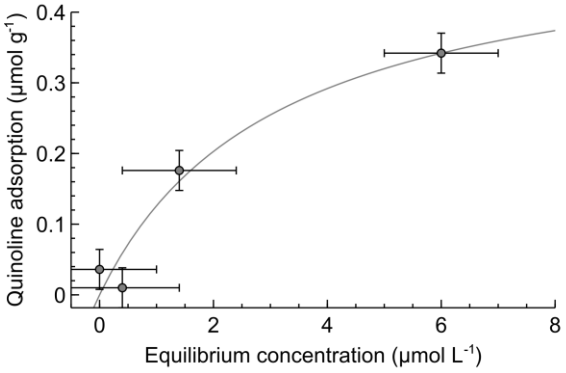

Figure S5. Quinoline adsorption over the 2 wt% Pd/$CaCO_3$ catalyst in hexane.

Confidence intervals for the Langmuir model fitting onto quinoline adsorption are broad with both the adsorption constant and the capacity poorly defined. The reason for the poorly defined values is that full surface coverage was not observed.

Table S2. 90% Confidence intervals of quinoline adsorption over the 2 wt% Pd/$CaCO_3$ catalyst.

	Best fit value	Confidence interval	
		Lower boundary	Higher boundary
K (L μmol^{-1})	0.32	0.00017	11.6
n_max (μmol g_{cat}^{-1})	0.52	0.308	120

SI5. Model of MBY hydrogenation over the alkene and alkyne active sites.

Figure shows the scheme of the reaction model that takes into account MBY into MBE hydrogenation over the alkyne sites followed by MBE to MBA hydrogenation over both the alkene and alkyne sites. The model assumes non-competitive adsorption of organic species and hydrogen as well as no adsorption of MBY over the alkene sites. Adsorption constants of alkyne over the alkyne sites were taken according to the value determined experimentally, while the adsorption constant of alkenes over the alkyne sites was considered to be significantly lower than that of alkynes – at a fixed value of 30 L mol^{-1}. The particular value plays a little role as long as it is significantly lower than MBY adsorption constant determined experimentally.

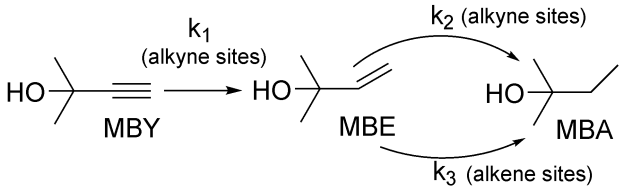

Figure S6. Scheme of the MBY hydrogenation model that considers alkyne and alkene adsorption sites.

Equations S22-S24 are obtained based on these assumptions and include n_{alkyne_sites} and n_{alkene_sites} are the numbers of alkyne and alkene adsorption sites determined by the adsorption measurements, K_{MBY} and K_{MBE} are the adsorption constants of MBY and MBE over the *alkyne* sites. The model assumes adsorption of the organic molecules over "ensembles" of several neighbouring Pd surface sites for simplicity. K_{MBY} was determined experimentally, while K_{MBE} was assumed to be significantly lower with the value of 10 L mol^{-1} (a factor of 5,000 lower than K_{MBY}). Hydrogenation of MBE over the alkene sites was considered as a zero-order reaction because no competition with MBY adsorption and high adsorption constant resulted in complete surface coverage.

$$r_1 = k_1 n_{alkyne\_sites} \frac{K_{MBY} C_{MBY}}{1 + K_{MBY} C_{MBY} + K_{MBE} C_{MBE}}, \quad (S22)$$

$$r_1 = k_2 n_{alkyne\_sites} \frac{K_{MBE} C_{MBE}}{1 + K_{MBY} C_{MBY} + K_{MBE} C_{MBE}}, \quad (S23)$$

$$r_3 = k_3 n_{alkene\_sites}. \quad (S24)$$

A Matlab program performed numerical integration of the reaction rates considering changes in MBY and MBE concentration described in equation S25-S27. Regression analysis performed adjusted only the apparent rate constants (k_1, k_2, k_3) to describe the experimental concentration profiles.

$$\frac{dC_{MBY}}{dt} = -r_1, \quad (S25)$$

$$\frac{dC_{MBE}}{dt} = r_1 - r_2 - r_3, \quad (S26)$$

$$\frac{dC_{MBA}}{dt} = r_2 + r_3, \quad (S27)$$

A sensitivity analysis of the model was performed – a pair of parameters was perturbed from its optimal value (the most accurate description of the experiment) and the effect on the weighed residual was analysed. It is worth pointing out that using statistical weighing (inversely proportional to experimental uncertainties) provided dimensionless residual values – the values independent of the concentration units.

Figure S shows the resulting sensitivity profiles which show a narrow region of parameters that describe the experimental concentration profiles. The sensitivity analysis can also show covariation of the parameters – the phenomenon where a change in one parameter may be compensated by a change in another one.

No significant covariation of the parameters can be observed which would have resulted in the formation of narrow valleys across the parameter space

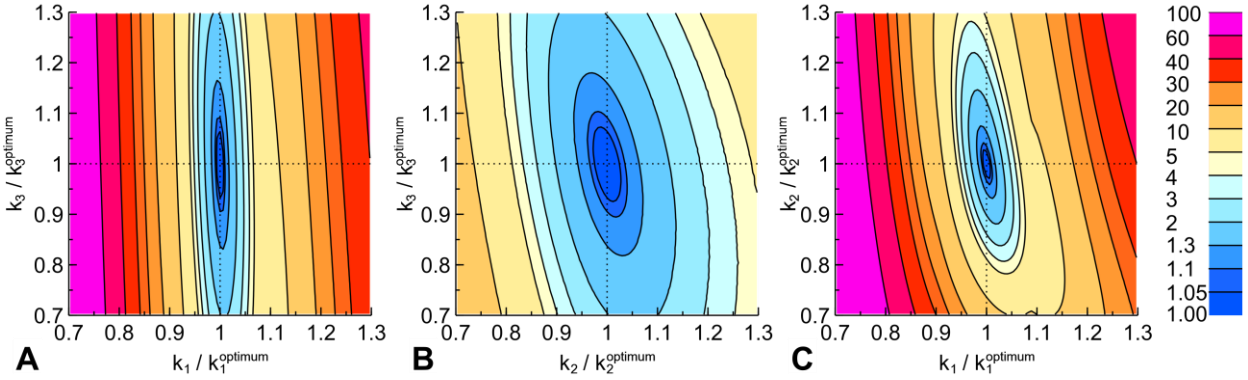

Figure S7. Sensitivity analysis – the effect of changing the model parameters away from the optimum onto the weighted sum of residuals.

SI6. DFT adsorption studies performed over the Pd surface

MBY and MBE molecules could adsorb on the Pd catalyst surface through different sites (Figure S). The initial adsorption could occur via the methyl group, oxygen or hydrogen atoms of the hydroxyl group and or the terminal CH group. Additionally, such adsorption could occur on top of a Pd atom, in between two Pd atoms, and on the hollow sites.

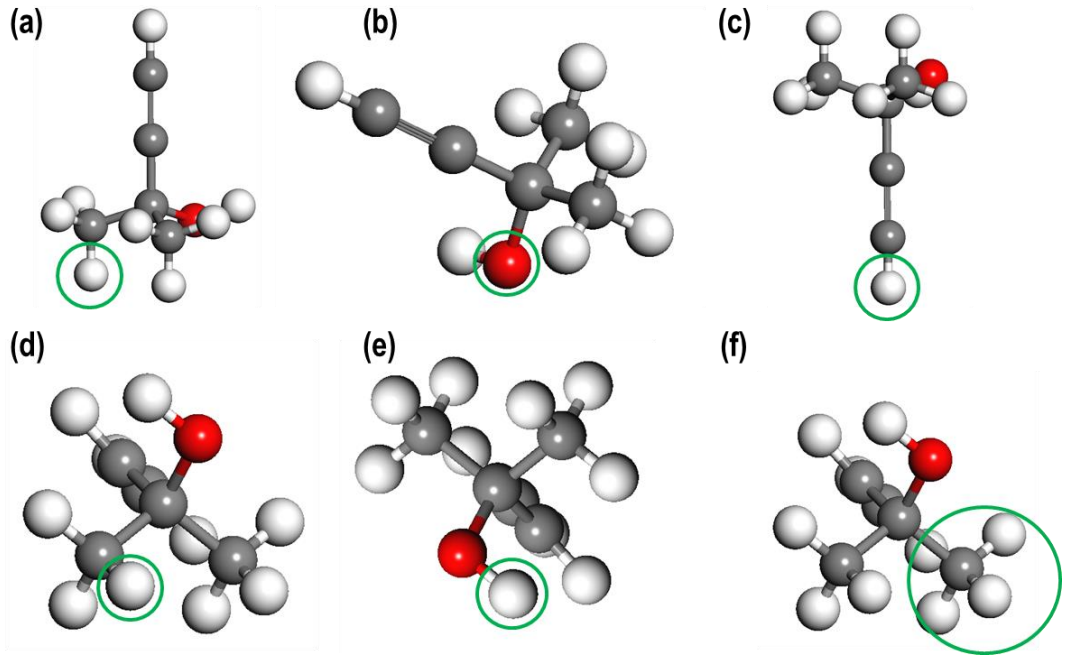

Figure S8. Possible adsorption positions of MBY (a) through the methyl group, (b) through the O-atom of the OH group, (c) adsorption through H of the CH. The of MBE adsorption (d) via all H on CH_3 group, (e) adsorption via H of the OH group and (f) via the CH_3 group. The green circles represent the H and O-atoms with respect to which the adsorption was considered.

To further quantify our observation, we investigate the area under the Pd *d*-orbital signatures for these two models using:

$$Area = \int_{-a}^{-b} D.dE,$$

where –a and –b are the lower and upper limit respectively for the overlapping region, D is the contribution of the *d*-orbital signatures and dE is the difference between two nearest energy levels. Our calculation shows that the area under the *d*-orbital signatures of the first, second and the third Pd atoms in MBY_O_Pd_{hollow} model are respectively, 0.244, 0.165 and 0.205 number of states (and a total of 0.615 number of states), which are higher than 0.111 number of states for MBE_OH_Pd_{bdg} model. Thus MBY model is more strongly adsorbed on the Pd(111) surface as compared to the MBE molecule.

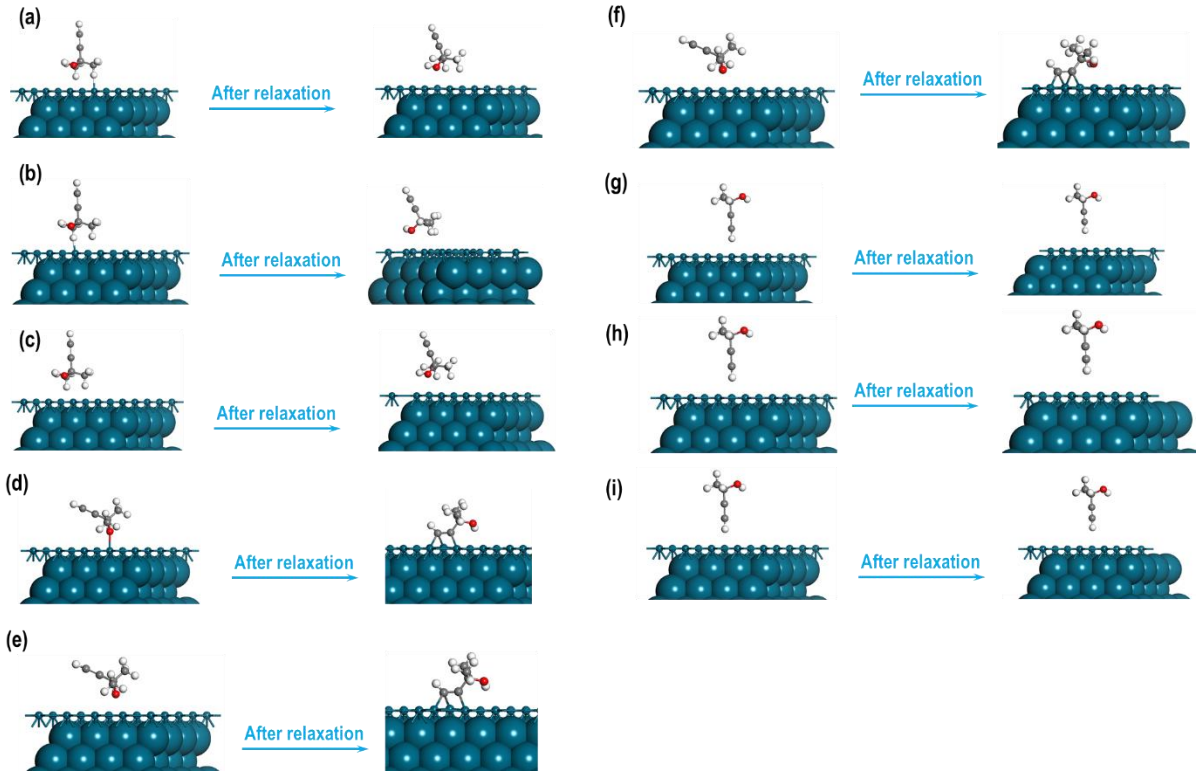

Figure S9. The optimised structures of (a) MBY_CH_3_Pd_{top}, (b) MBY_CH_3_Pd_{bdg}, (c) MBY_CH_3_Pd_{hollow}, (d) MBY_O_Pd_{top}, (e) MBY_O_Pd_{bdg}, (f) MBY_O_Pd_{hollow}, (g) MBY_CH_Pd_{top}, (h) MBY_CH_Pd_{Bdg}, and (i) MBY_CH_Pd_{hollow}.

References

[1] J.S. Alper, R.I. Gelb, Standard errors and confidence intervals in nonlinear regression: comparison of Monte Carlo and parametric statistics, J. Phys. Chem. 94 (1990) 4747–4751. https://doi.org/10.1021/j100374a068.

[2] G. Kresse, J. Hafner, Ab initio molecular dynamics for liquid metals, Phys. Rev. B. 47 (1993) 558–561. https://doi.org/10.1103/PhysRevB.47.558.

[3] G. Kresse, J. Hafner, Ab initio molecular-dynamics simulation of the liquid-metal--amorphous-semiconductor transition in germanium, Phys. Rev. B. 49 (1994) 14251–14269.

https://doi.org/10.1103/PhysRevB.49.14251.

[4] G. Kresse, From ultrasoft pseudopotentials to the projector augmented-wave method, Phys. Rev. B. 59 (1999) 1758–1775. https://doi.org/10.1103/PhysRevB.59.1758.

[5] P.E. Blöchl, Projector augmented-wave method, Phys. Rev. B. 50 (1994) 17953–17979. https://doi.org/10.1103/PhysRevB.50.17953.

[6] S.M. Rogers, C.R.A. Catlow, C.E. Chan-Thaw, A. Chutia, N. Jian, R.E. Palmer, M. Perdjon, A. Thetford, N. Dimitratos, A. Villa, P.P. Wells, Tandem Site- and Size-Controlled Pd Nanoparticles for the Directed Hydrogenation of Furfural, ACS Catal. 7 (2017) 2266–2274. https://doi.org/10.1021/acscatal.6b03190.

[7] G. Makov, M. Payne, Periodic boundary conditions in ab initio calculations, Phys. Rev. B. 51 (1995) 4014–4022. https://doi.org/10.1103/PhysRevB.51.4014.

[8] J. Neugebauer, M. Scheffler, Adsorbate-substrate and adsorbate-adsorbate interactions of Na and K adlayers on Al(111), Phys. Rev. B. 46 (1992) 16067–16080. https://doi.org/10.1103/PhysRevB.46.16067.

[9] S. Grimme, J. Antony, S. Ehrlich, H. Krieg, A consistent and accurate ab initio parametrization of density functional dispersion correction (DFT-D) for the 94 elements H-Pu, J. Chem. Phys. 132 (2010). https://doi.org/10.1063/1.3382344.

[10] E.K. Dann, E.K. Gibson, R.H. Blackmore, C.R.A. Catlow, P. Collier, A. Chutia, T.E. Erden, C. Hardacre, A. Kroner, M. Nachtegaal, A. Raj, S.M. Rogers, S.F.R. Taylor, P. Thompson, G.F. Tierney, C.D. Zeinalipour-Yazdi, A. Goguet, P.P. Wells, Structural selectivity of supported Pd nanoparticles for catalytic NH 3 oxidation resolved using combined operando spectroscopy, Nat. Catal. 2 (2019) 157–163. https://doi.org/10.1038/s41929-018-0213-3.

[11] Y. Bai, N. Cherkasov, S. Huband, D. Walker, R. Walton, E. Rebrov, Highly Selective Continuous Flow Hydrogenation of Cinnamaldehyde to Cinnamyl Alcohol in a Pt/SiO2 Coated Tube Reactor, Catalysts. 8 (2018) 1–18. https://doi.org/10.3390/catal8020058.

[12] M. Crespo-Quesada, M. Grasemann, N. Semagina, A. Renken, L. Kiwi-Minsker, Kinetics of the solvent-free hydrogenation of 2-methyl-3-butyn-2-ol over a structured Pd-based catalyst, Catal. Today. 147 (2009) 247–254. https://doi.org/10.1016/j.cattod.2008.09.035.

[13] N. Cherkasov, Liquid-phase adsorption: Common problems and how we could do better, J. Mol. Liq. 301 (2020) 1–8. https://doi.org/10.1016/j.molliq.2019.112378.

[14] B.H. Stitt, M. Marigo, S. Wilkinson, T. Dixon, How Good is Your Model ?, Johnson Matthey Technol. Rev. 59 (2015) 74–89. https://doi.org/10.1595/205651315X686804 JOHNSON.

[15] N. Cherkasov, T. Vazhnova, D.B. Lukyanov, Quantitative infra-red studies of Brønsted acid sites in zeolites: Case study of the zeolite mordenite, Vib. Spectrosc. 83 (2016) 170–179. https://doi.org/10.1016/j.vibspec.2016.02.002.

[16] L. Vattuone, Y.Y. Yeo, R. Kose, D.A. King, Energetics and kinetics of the interaction of acetylene and ethylene with Pd {100} and Ni {100}, Surf. Sci. 447 (2000) 1–14. http://www.ncbi.nlm.nih.gov/entrez/query.fcgi?db=pubmed&cmd=Retrieve&dopt=AbstractPlus&list_uids=3866405211267739216related:UC5V9w07qDUJ%5Cnhttp://linkinghub.elsevier.com/retrieve/pii/S0039602899011929.